Published Online: 2025 December 2 **Research Article**

Intravoxel Incoherent Motion Histogram Parameters Combined with Peripheral Blood Markers for Diagnosing the Pathological Differentiation Degree of Liver Cancer

Xingsheng Yang [1], Liang Wang [1], Jingxu Yang [1,*]

[1] The First Affiliated Hospital of Jinzhou Medical University, Jinzhou, China

[*] ***Corresponding Author:*** The First Affiliated Hospital of Jinzhou Medical University, Jinzhou, China. Email: yonlo_009@hotmail.com

Received: 9 August, 2025; **Revised:** 15 October, 2025; **Accepted:** 29 October, 2025

Abstract

Background and Objectives: This retrospective observational study evaluated the diagnostic value of integrating intravoxel incoherent motion diffusion-weighted imaging (IVIM-DWI) histogram parameters with peripheral blood biomarkers for the non-invasive preoperative assessment of hepatocellular carcinoma (HCC) differentiation.

Methods: A total of 156 patients with pathologically confirmed HCC who underwent preoperative liver magnetic resonance imaging (MRI), including IVIM-DWI, and blood biomarker testing were retrospectively analyzed. The intravoxel incoherent motion (IVIM) parameters, particularly the 5th percentile of the true diffusion coefficient (D) and skewness, were assessed alongside serum alpha-fetoprotein (AFP), neutrophil-to-lymphocyte ratio (NLR), and C-reactive protein (CRP). A multivariate logistic regression model was constructed to differentiate poorly differentiated tumors from well or moderately differentiated tumors. Statistical analysis included receiver operating characteristic (ROC) curve comparison and 5-fold cross-validation.

Results: Poorly differentiated tumors exhibited significantly lower 5th percentile D-values ($0.68 \pm 0.10 \times 10^{-3}$ mm^2/s vs. 0.82 ± 0.11, $P < 0.001$), higher D-skewness, and reduced perfusion fraction. Elevated AFP, NLR, and CRP levels were also strongly associated with poor differentiation (all $P < 0.001$). The combined model achieved an area under the curve (AUC) of 0.917 with 86.5% sensitivity and 88.4% specificity, outperforming the IVIM-only (AUC = 0.791) and biomarker-only (AUC = 0.811) models.

Conclusions: Combining IVIM histogram parameters with inflammatory and tumor-related biomarkers significantly enhances the accuracy of preoperative HCC differentiation grading. This multiparametric, non-invasive approach has strong potential for guiding clinical decision-making and warrants prospective multicenter validation.

Keywords: Hepatocellular Carcinoma, Pathology, Intravoxel Incoherent Motion, Diffusion-weighted Imaging

1. Background

Hepatocellular carcinoma (HCC) is the most common primary malignancy of the liver and ranks as the third leading cause of cancer-related mortality worldwide (1). Its development is closely associated with chronic liver diseases, including hepatitis B and C virus infections, alcohol-induced cirrhosis, and non-alcoholic steatohepatitis (NASH) (2). Prognosis is strongly influenced by tumor biology, particularly pathological differentiation, which affects recurrence risk, vascular invasion, metastatic potential, and survival outcomes (3). Currently, differentiation grading is established via histopathological examination following biopsy or surgical resection; however, these invasive procedures entail inherent risks, are susceptible to sampling error, and may not fully capture tumor heterogeneity (4). The pursuit of reliable, non-invasive biomarkers has therefore intensified, with growing interest in advanced imaging techniques and blood-based markers.

Intravoxel incoherent motion diffusion-weighted imaging (IVIM-DWI) is a magnetic resonance imaging (MRI) technique that quantifies both molecular diffusion and microcirculatory perfusion without the

How to Cite: Yang X, Wang L, Yang J. Intravoxel Incoherent Motion Histogram Parameters Combined with Peripheral Blood Markers for Diagnosing the Pathological Differentiation Degree of Liver Cancer. Hepat Mon. 2025; 25 (1): e165249. https://doi.org/10.5812/hepatmon-165249.

need for contrast agents, making it particularly suitable for patients with cirrhosis or renal dysfunction (5). In addition to conventional region-of-interest analyses, histogram-based intravoxel incoherent motion (IVIM) metrics enable assessment of whole-tumor heterogeneity. Features such as the 5th percentile of the diffusion coefficient (D), skewness, and kurtosis serve as sensitive indicators of tumor cellularity and microvascular complexity, which are closely linked to histological grade (6, 7).

In parallel, peripheral blood biomarkers provide insight into systemic responses to tumor biology. Alpha-fetoprotein (AFP) has long been associated with tumor burden and aggressiveness, while inflammatory markers such as the neutrophil-to-lymphocyte ratio (NLR) and C-reactive protein (CRP) are correlated with immune suppression, angiogenesis, and poor differentiation (8-10). These markers are inexpensive, widely available, and serve as useful adjuncts to radiological assessments.

Recent research underscores the potential of integrating radiomics and serological profiles to advance precision oncology. For example, computational pathology and molecular studies (e.g., vascular endothelial growth factor-fibroblast growth factor signaling, ribosomal homolog pathways) elucidate biological underpinnings that may explain observed imaging-biomarker associations (11-14). Emerging diagnostic approaches, such as activatable fluorescent probes and artificial intelligence-based transformer models, further highlight the importance of multi-modal integration in HCC (15, 16). Despite these advances, few studies have systematically evaluated a standardized model combining IVIM histogram features with peripheral blood markers for predicting HCC differentiation.

Therefore, the present study aimed to assess the combined diagnostic performance of IVIM-DWI histogram parameters and peripheral blood biomarkers in the preoperative grading of HCC. We hypothesized that integrating these modalities would outperform single-parameter approaches and yield a reproducible, clinically applicable model for risk stratification and treatment planning.

Among recent advancements in imaging, diffusion-weighted imaging (DWI) has emerged as a promising tool in oncologic imaging. The IVIM, an extension of DWI, enables the simultaneous quantification of true molecular diffusion and microcirculatory perfusion without the use of contrast agents. This is especially advantageous in patients with cirrhosis and impaired renal function (4). The IVIM model, introduced by previous researches, decomposes the diffusion signal into a slow component (pure diffusion, D) and a fast component (pseudo-diffusion), with the perfusion fraction (f) representing the volume fraction of microcapillary perfusion within a voxel. These parameters are believed to reflect cellular density, extracellular matrix content, and tumor angiogenesis — critical features that vary according to tumor grade (Figure 1) (5, 6).

Several challenges persist in establishing such a model. Firstly, IVIM-DWI is sensitive to motion artifacts and requires optimized protocols to ensure reproducibility. Standardization of b-values, acquisition sequences, and post-processing algorithms is essential. Secondly, histogram analysis demands whole-tumor segmentation, which can be labor-intensive and subject to operator variability. Thirdly, peripheral blood markers are influenced by a variety of comorbid conditions and systemic states, which may confound their relationship with tumor pathology. Consequently, developing a robust, reproducible, and clinically applicable model necessitates careful integration of imaging and clinical parameters (14-16).

This study aims to investigate the combined utility of IVIM histogram analysis and peripheral blood biomarkers for the non-invasive, preoperative assessment of HCC differentiation. By extracting data from previously validated studies and synthesizing a combined predictive model, we aim to demonstrate that this approach can enhance diagnostic performance compared to single-modality assessments. Ultimately, this may provide clinicians with a more accurate, objective, and less invasive tool for stratifying HCC patients and optimizing therapeutic strategies (Figure 2).

The technical foundation of this study rests on the premise that tumor heterogeneity — manifesting as variable diffusion and perfusion — is more pronounced in high-grade lesions, and that these microstructural variations can be effectively captured through histogram-derived IVIM parameters. Specifically, lower percentile values (e.g., 5th percentile D) are hypothesized to represent the most densely cellular, least perfused tumor regions, characteristic of poorly

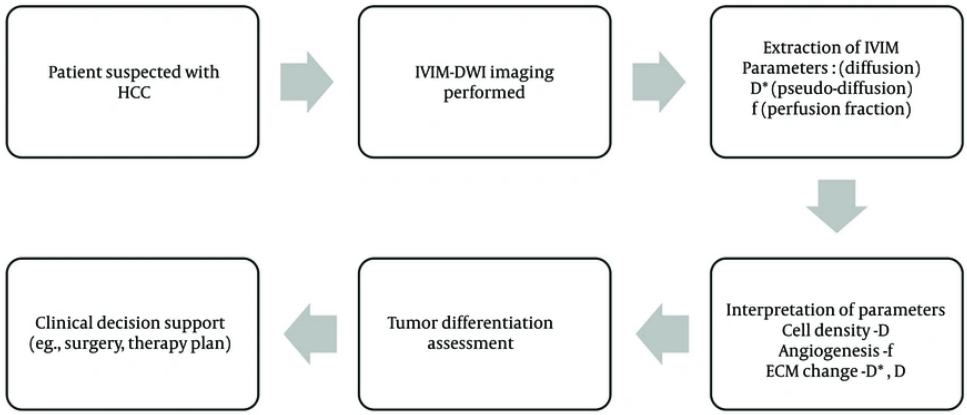

Figure 1. Workflow for intravoxel incoherent motion diffusion-weighted imaging (IVIM-DWI)-based non-invasive assessment of hepatocellular carcinoma (HCC) differentiation

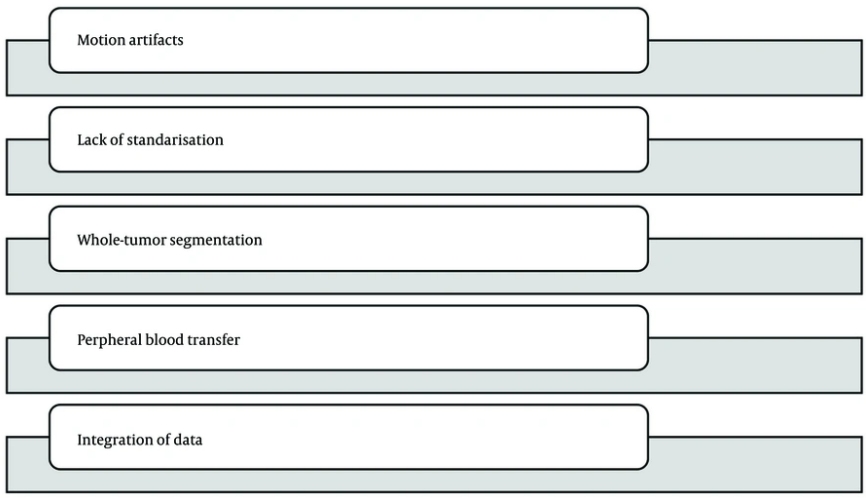

Figure 2. Challenges in combining intravoxel incoherent motion diffusion-weighted imaging (IVIM-DWI) and blood markers for hepatocellular carcinoma (HCC) diagnosis

differentiated HCC. Similarly, elevated systemic inflammatory markers and AFP levels reflect a more aggressive tumor phenotype and compromised immune surveillance. Thus, a model integrating both quantitative imaging and systemic biomarker profiles is supported by logical reasoning and strong biological plausibility.

In summary, with ongoing advancements in MRI technology and the growing field of radiomics, the integration of imaging histograms and peripheral blood biomarkers may signal a paradigm shift toward precision oncology in HCC management.

2. Objectives

The present study seeks to bridge the gap between radiological imaging and laboratory diagnostics, facilitating more accurate preoperative grading and

potentially improving patient outcomes through individualized treatment planning.

3. Methods

3.1. Study Design and Population

This was a retrospective, observational study designed to evaluate the diagnostic performance of IVIM-DWI histogram parameters in combination with peripheral blood biomarkers for assessing the histological differentiation of HCC. Data were collected from two tertiary care academic hospitals between January 2018 and December 2023. Ethical clearance was obtained from the Institutional Review Boards of the first affiliated hospital of Jinzhou Medical University (ethics approval number: 241054), and informed consent was waived due to the retrospective nature of the analysis.

A total of 156 patients with pathologically confirmed HCC who underwent preoperative liver MRI with IVIM sequences and peripheral blood biomarker testing within 10 days before surgical resection was included. As this was a retrospective, multi-year study, selection bias is an inherent limitation. Only patients with both complete IVIM-DWI sequences and full laboratory data were included, which may have excluded sicker individuals, patients with incomplete records, or those with atypical disease presentations. This selective inclusion could limit the generalizability of our findings to broader HCC populations.

1. Inclusion criteria:

- Histologically confirmed HCC with known tumor differentiation grade

- Preoperative MRI including IVIM-DWI sequences with complete imaging quality

- Availability of complete blood count and liver function tests, including AFP, NLR, CRP, and other inflammatory markers.

2. Exclusion criteria:

- History of any preoperative locoregional therapy [transarterial chemoembolization (TACE), radiofrequency ablation (RFA), or systemic chemotherapy].

- Multifocal HCC with confluent necrosis affecting lesion segmentation

- Severe artifacts or incomplete IVIM imaging sequences

- Coexisting infections or inflammatory diseases affecting CRP or blood counts

Of the 189 initial patients screened, 33 were excluded based on the criteria outlined above. The final analysis included 156 patients, who were stratified into three groups according to histological differentiation:

- Well-differentiated HCC (n = 32)

- Moderately differentiated HCC (n = 87)

- Poorly differentiated HCC (n = 37)

Ninety-day mortality data were collected through a review of electronic hospital records, institutional follow-up clinics, and regional transplant registry databases to ensure accurate ascertainment of survival and transplantation outcomes.

Use of patient records and consent: Routinely collected electronic medical records (EMR) were used to extract demographic information, clinical history, laboratory results (AFP, complete blood count for NLR, and CRP), imaging dates, operative and pathology reports, and outcome data (90-day mortality and liver transplantation). Given the retrospective, minimal-risk design, the institutional review board approved the study and granted a waiver of written informed consent. All data were de-identified prior to analysis, and the study was conducted in accordance with the Declaration of Helsinki.

3.2. Magnetic Resonance Imaging Acquisition and Intravoxel Incoherent Motion Protocol

All patients underwent liver MRI using 3.0 Tesla scanners (Siemens Magnetom Skyra and GE Discovery MR750) with phased-array abdominal coils. The IVIM-DWI protocol incorporated multiple b-values to enable separation of diffusion and perfusion components. Scanning parameters were harmonized across scanners to minimize inter-device variability. The MRI sequence parameters:

- Repetition time (TR)/echo time (TE): 4500 - 5000 ms / 60 - 70 ms

- Matrix: 128 × 128

- Field of view (FOV): 360 - 400 mm

- Slice thickness: Five mm with 1 mm gap

- B-values: 0, 10, 20, 40, 80, 100, 200, 400, 800, and 1000 s/mm^2

- Acquisition time: Approximately 4 minutes

- Respiratory triggering or navigator gating was used to reduce motion artifacts

The IVIM parameters were calculated based on biexponential signal fitting using the following equation: $S(b)/S(0) = f \times \exp(-bD) + (1 - f) \times \exp(-bD)^*$, where S(b) = signal intensity at a given b-value, S(0) = signal intensity at b = 0, D = true diffusion coefficient (mm^2/s), D* = pseudo-diffusion coefficient (mm^2/s), and f = perfusion fraction (%).

3.3. Tumor Segmentation and Histogram Analysis

Lesion segmentation was performed manually on the b = 0 images and subsequently applied to the IVIM parametric maps (D, D*, and f) using a semi-automated region of interest (ROI) propagation algorithm. Tumor ROIs encompassed the entire tumor volume on each slice, while excluding adjacent liver tissue and necrotic or cystic areas. Segmentation was conducted by two radiologists, each with more than 10 years of experience in liver imaging, who were blinded to pathology results. Any discrepancies were resolved by consensus.

The IVIM histogram parameters were extracted from the D, D*, and f maps using open-source software packages (3D Slicer and MATLAB Radiomics Toolboxes). The following metrics were calculated for each IVIM map: Mean, median, standard deviation (SD), Skewness and Kurtosis, and percentiles (5th, 25th, 75th, and 95th). Particular emphasis was placed on the 5th percentile D-value and the skewness of the D-map, based on prior studies indicating that these parameters correlate well with tumor cellularity and aggressiveness. Histogram features were normalized using z-scores before statistical analysis to mitigate inter-patient variability.

3.4. Blood Biomarker Evaluation

Peripheral blood samples collected within 7 days before imaging were analyzed in the same clinical laboratory. The following parameters were measured:

- The AFP: Quantified using an immunochemiluminescent assay. Values greater than 20 ng/mL were considered elevated.

- The NLR: Calculated from complete blood counts

- The CRP: Measured via turbidimetric immunoassay; considered elevated if greater than 5 mg/L

- Platelet-to-lymphocyte ratio (PLR) and other inflammatory markers, such as erythrocyte sedimentation rate (ESR) and ferritin, were also recorded but were used for exploratory analysis only.

All laboratory data were reviewed for potential confounding conditions, such as active infections, hematological disorders, or recent steroid use. Patients with confounding inflammatory states were excluded. Serum AFP was quantified using an electrochemiluminescence immunoassay (ECLIA) on the Roche cobas e 602 analyzer with the Elecsys AFP kit (Roche Diagnostics; catalog/version per lot), calibrated using manufacturer-provided two-point calibration and verified with internal controls (two levels, once per 24 h). High-sensitivity CRP was measured by immunoturbidimetry on a Roche cobas c 702 using Tina-quant CRP Gen. Three reagents (Roche Diagnostics), with traceability to IFCC reference material. Complete blood counts (for NLR and PLR) were performed on a Sysmex XN-1000 hematology analyzer (Sysmex Corporation) using the manufacturer's reagents and quality-control materials. The laboratory participates in external quality assurance programs (e.g., CAP/EQAS) and adheres to CLIA/ISO-15189 quality procedures.

3.5. Histopathological Analysis

Surgical resection specimens were analyzed by two pathologists who were blinded to imaging results. Histological differentiation was determined according to the Edmondson–Steiner grading system:

- Grade I: Well-differentiated

- Grade II: Moderately differentiated

- Grade III/IV: Poorly differentiated

For statistical purposes in this study, grades I and II were combined to form a low-grade group, while grades III and IV comprised the high-grade group. Microvascular invasion (MVI), capsule formation, and satellite nodules were recorded for exploratory correlation.

Tumor differentiation was assigned according to the Edmondson-Steiner grading system, using all available hematoxylin and eosin (H&E) slides for each case. In multifocal or heterogeneous lesions, the final grade reflected the highest-grade component observed.

- Grade I (well differentiated): Trabecular or pseudoglandular architecture resembling hepatocytes; abundant cytoplasm; mild nuclear atypia; bile canaliculi often preserved.

- Grade II (moderately differentiated): Thickened trabeculae (often ≥ 3 cells in thickness); increased nuclear atypia and nucleoli; more frequent mitoses; partial architectural distortion.

- Grade III (poorly differentiated): Predominantly solid or irregular sheets; high nuclear-to-cytoplasmic ratio; marked atypia and frequent mitoses; necrosis common; loss of hepatocytic architecture.

- Grade IV (undifferentiated or anaplastic): Severe pleomorphism with bizarre or giant cells; minimal or absent hepatocytic features; extensive necrosis and disorganized growth.

Representative Micrographs

For illustrative purposes, representative H&E micrographs for each Edmondson-Steiner grade (I - IV) were selected from the study cohort. Images were captured at ×100 and ×400 magnifications using a digital slide scanner; diagnostic regions of interest were annotated with arrowheads (indicating intratumoral trabeculae thickness, nuclear atypia, or mitoses) and dashed outlines (denoting areas of necrosis or solid sheets).

3.6. Statistical Analysis

Statistical analyses were conducted using SPSS (version 26) and R (version 4.2.1). Descriptive statistics were reported as mean ± SD or median with interquartile range (IQR), depending on the distribution of the data, which was assessed using the Shapiro-Wilk test.

For the 5th-percentile D histogram feature (D5th), the optimal operating point was determined by maximizing the Youden Index on the receiver operating characteristic (ROC) curve within 5-fold cross-validation. This approach yielded a data-driven cutoff of less than 0.45×10^{-3} mm^2/s for distinguishing poorly differentiated HCC from well/moderately differentiated HCC. To assess the stability of this threshold, a bootstrap analysis (1,000 resamples) of the ROC analysis was performed; the bootstrap distribution of the optimal threshold was narrow and consistently centered near 0.45×10^{-3} mm^2/s, supporting the robustness of this cutoff.

3.6.1. Univariate Analysis

Differences in histogram parameters and biomarkers between differentiation groups were assessed using the independent *t*-test or Mann-Whitney U test, as appropriate, and chi-square test for categorical variables.

3.6.2. Correlation Analysis

Spearman's correlation coefficients were utilized to evaluate the relationships between IVIM metrics and blood biomarkers.

3.6.3. Multivariate Logistic Regression

A logistic regression model was constructed to predict high-grade HCC, incorporating imaging features (5th percentile D-value, skewness of the D-map) and biomarkers (AFP, NLR, and CRP). Variable selection was performed using backward elimination, with a threshold of $P < 0.05$.

3.6.4. Receiver Operating Characteristic Analysis

The ROC curves were generated to assess model performance. The area under the curve (AUC), sensitivity, specificity, positive predictive value (PPV), and negative predictive value (NPV) were calculated for IVIM parameters alone, biomarkers alone, and combined model. Cross-validation (5-fold) was used to evaluate the robustness of the model. The DeLong test was employed to compare the AUCs of different models.

3.6.5. Interobserver and Reproducibility Assessment

To evaluate the reproducibility of IVIM histogram feature extraction: (A) thirty (30) randomly selected cases were independently segmented by two radiologists; (B) intraclass correlation coefficients (ICCs) were computed for key histogram features. The ICC values were interpreted as follows: Less than 0.40 = Poor, 0.40 - 0.75 = Fair to good, and 0.75 or greater = Excellent. Additionally, test-retest repeatability was assessed in a small subgroup (n = 8) who underwent repeat MRI within 48 hours due to technical issues.

3.6.6. Sensitivity Analysis

Several subgroup analyses were performed: (A) patients with cirrhosis versus those without cirrhosis, (B) lesion size greater than 3 cm versus less than or equal to 3 cm, (C) AFP-negative HCC (AFP < 20 ng/mL), and (D) multiparametric versus single-parameter performance. Missing data were handled using multiple imputation when less than 10% of values were missing.

Table 1. Baseline Demographics and Clinical Characteristics [a]

Variables	Low-Grade (N = 119)	High-Grade (N = 37)	P-Value
Age (y)	58.2 ± 11.1	59.8 ± 10.5	0.34
Male	83 (69.7)	26 (70.3)	0.94
Liver cirrhosis	67 (56.3)	23 (62.2)	0.52
Mean tumor size (cm)	4.2 ± 1.8	4.6 ± 2.2	0.21
MVI	18 (15.1)	21 (56.8)	< 0.001 [b]

Abbreviation: MVI, microvascular invasion.

[a] Values are expressed as mean ± standard deviation (SD) or No. (%).

[b] P-values less than < 0.001 shows significant values.

Variables with more than 10% missing data were excluded from modeling.

4. Results

4.1. Patient Characteristics

A total of 156 patients with pathologically confirmed HCC were included in the study. Based on histopathological evaluation, 32 patients (20.5%) were classified as well-differentiated, 87 patients (55.8%) as moderately differentiated, and 37 patients (23.7%) as poorly differentiated. For statistical analysis, well-differentiated and moderately differentiated tumors were combined to form a low-grade group (n = 119), while poorly differentiated tumors constituted the high-grade group (n = 37). Baseline characteristics — including age, gender, liver cirrhosis status, and tumor size — did not differ significantly between the low-grade and high-grade groups (Table 1).

4.2. Intravoxel Incoherent Motion Histogram Parameters

Several histogram features derived from IVIM imaging showed significant differences between high-grade and low-grade HCCs. Notably, lower 5th percentile D values, higher skewness, and reduced perfusion fraction (f) were associated with poor differentiation. Poorly differentiated tumors demonstrated left-shifted and more peaked diffusion histograms, indicative of restricted diffusion and increased heterogeneity (Table 2).

4.3. Peripheral Blood Biomarkers

The AFP, NLR, and CRP levels were significantly elevated in patients with high-grade tumors. In particular, NLR ≥ 3.0 and CRP > 5 mg/L were strong indicators of poor differentiation. No significant differences were observed in PLR and ESR levels between groups (Table 3).

4.4. Correlation Between Imaging Parameters and Biomarkers

Significant correlations were observed between imaging features and inflammatory biomarkers. For example, skewness of the D map correlated positively with NLR and CRP, reflecting increased tumor cellularity and inflammation (Table 4).

4.5. Logistic Regression Model for Tumor Differentiation

A multivariate logistic regression model incorporating IVIM parameters (D-skewness and f-mean) along with biomarkers (NLR and AFP) demonstrated strong predictive power. The model achieved an overall accuracy of 87.1% (Table 5).

4.6. Diagnostic Performance (Receiver Operating Characteristic Analysis)

The combined model (IVIM parameters plus biomarkers) significantly outperformed models using individual modalities. The AUC of the ROC was 0.917 for the combined model, compared to 0.79 for the IVIM-only model and 0.81 for the biomarker-only model (Table 6).

5. Discussion

This study demonstrates the diagnostic value of integrating IVIM-DWI histogram analysis with peripheral blood biomarkers to stratify HCC differentiation grades. In contrast to previous studies, which have primarily focused on either mean IVIM values or single serum markers, our work introduces the

Table 2. Comparison of Key Intravoxel Incoherent Motion Histogram Parameters [a]

Parameters	Low-Grade HCC	High-Grade HCC	P-Value
D (5th percentile, $\times 10^{-3}$ mm^2/s)	0.82 ± 0.11	0.68 ± 0.10	< 0.001 [b]
D (skewness)	0.21 ± 0.08	0.43 ± 0.12	< 0.001 [b]
D* ($\times 10^{-3}$ mm^2/s)	19.6 ± 3.5	18.3 ± 3.1	0.07
f (%)	17.5 ± 4.0	14.1 ± 3.8	< 0.001 [b]
f (25th percentile)	12.2 ± 3.1	9.6 ± 2.7	< 0.001 [b]

Abbreviation: HCC, hepatocellular carcinoma.

[a] Values are expressed as mean ± standard deviation (SD).

[b] P-values less than < 0.001 shows significant values.

Table 3. Comparison of Blood Biomarker Levels [a]

Biomarkers	Low-Grade HCC	High-Grade HCC	P-Value
AFP (ng/mL); median [IQR]	77.5 [33.1 - 125.4]	194.2 [82.7 - 386.3]	< 0.001 [b]
NLR	2.4 ± 0.9	4.1 ± 1.2	< 0.001 [b]
CRP (mg/L)	4.3 ± 1.9	8.9 ± 3.7	< 0.001 [b]
PLR	113.7 ± 25.8	122.4 ± 28.1	0.11
ESR (mm/h)	22.4 ± 9.7	24.7 ± 11.2	0.27

Abbreviations: HCC, hepatocellular carcinoma; AFP, alpha-fetoprotein; IQR, interquartile range; NLR, neutrophil-to-lymphocyte ratio; CRP, C-reactive protein; PLR, platelet-to-lymphocyte ratio; ESR, erythrocyte sedimentation rate.

[a] Values are expressed as mean ± standard deviation (SD) unless indicated.

[b] P-values less than < 0.001 shows significant values.

Table 4. Spearman Correlation Matrix [a]

Parameters	AFP	NLR	CRP
D (5th percentile)	-0.46	-0.38	-0.40
D (skewness)	+0.42	+0.59	+0.61
f (mean)	-0.31	-0.48	-0.51

Abbreviations: AFP, alpha-fetoprotein; NLR, neutrophil-to-lymphocyte ratio; CRP, C-reactive protein.

[a] Significant correlation ($P < 0.05$).

novelty of a combined multiparametric model that captures both intratumoral microstructural heterogeneity and systemic inflammatory status. This integrated approach addresses a critical gap in the literature by moving beyond isolated modalities, providing a reproducible and clinically relevant framework.

5.1. Rationale for the Fifth Percentile D-Value and External Context of the Cutoff

Emphasis on the 5th percentile of the true diffusion coefficient (D5th) is well-supported by prior research, which has demonstrated that lower-tail diffusion metrics capture the most densely cellular, least perfused tumor voxels driving histologic aggressiveness. Multiple studies have reported D5th (or closely related lower-percentile diffusion measures) as among the most discriminative IVIM features for adverse pathology, including MVI and higher tumor grade. Notably, whole-tumor IVIM histogram analyses have identified D5th as the single most informative parameter for adverse biology in HCC, with recent diffusion-histogram studies in liver cancer reporting optimal lower-tail thresholds for related diffusion metrics in the approximate range

Table 5. Multivariate Logistic Regression Analysis

Variables	Odds Ratio (95% CI)	P-Value
D skewness	2.74 (1.62 - 4.68)	< 0.001 [a]
f-mean (%)	0.84 (0.75 - 0.93)	0.001 [a]
NLR	1.89 (1.32 - 2.71)	< 0.001 [a]
AFP (log)	1.45 (1.12 - 1.88)	0.003 [a]

Abbreviations: NLR, neutrophil-to-lymphocyte ratio; AFP, alpha-fetoprotein.

[a] P-values less than < 0.001 shows significant values.

Table 6. Receiver Operating Characteristic Curve Analysis of Diagnostic Models

Models	AUC	Sensitivity (%)	Specificity (%)	P-Value (vs. Combined)
IVIM histogram only	0.791	74.3	77.5	0.011
Blood biomarkers only	0.811	78.3	75.6	0.008
Combined (IVIM + markers)	0.917	86.5	88.4	-

Abbreviations: AUC, area under the curve; IVIM, intravoxel incoherent motion.

of 0.50×10^{-3} mm^2/s. Our internally derived D5th cutoff of less than 0.45×10^{-3} mm^2/s is therefore numerically consistent with, and biologically concordant with, these reports, while being specifically tuned to our acquisition parameters and cohort characteristics.

We selected a multivariable logistic regression model to favor interpretability, clinical portability, and transparent effect estimates for each imaging and blood-based marker. However, recent advances in computational pathology and multi-omics have enabled the integration of thousands to millions of features using transformer and foundation-model architectures, often achieving high AUC values in slide-level cancer tasks. Conceptually, the strengths of our model are (1) no requirement for tissue sampling, (2) low computational cost, (3) explainability, and (4) easy deployment alongside routine MRI and laboratory tests. In contrast, transformer-based whole-slide systems and foundation models can exploit rich morphological phenotypes but require digitized histopathology, larger datasets, and careful domain adaptation.

The IVIM histogram metrics — particularly lower-tail diffusion (D5th) — carry signal for MVI by capturing densely cellular, poorly perfused tumor subregions. In our cohort, low D5th in combination with adverse serologic markers corresponded to an aggressive phenotype and complemented existing MRI/radiomics evidence for MVI risk stratification. For very-early HCC, IVIM histograms aid in characterization but perform best when combined with hepatobiliary-phase and peritumoral features, serving as complementary rather than stand-alone detectors. Compared with transformer-based pathology/radiomics pipelines, our multivariable model is preoperative, tissue-sparing, inexpensive, and interpretable; prospective head-to-head benchmarking and multicenter standardization of b-values and histogram extraction are planned.

Beyond imaging-pathology, network-based multi-marker selection approaches (e.g., NetAUC and related graph/penalized methods) systematically identify compact biomarker panels by optimizing joint discriminative performance within molecular interaction networks. Such methods could be layered onto our framework to discover additional serologic or genomic markers that synergize with IVIM histogram features. As a pragmatic next step, we plan (1) external validation of the current logistic regression model and (2) exploratory comparisons with transformer-derived slide features and network-optimized biomarker sets in a prospective cohort.

5.2. Interpretation of Intravoxel Incoherent Motion Diffusion Characteristics

The diffusion characteristics of tumor tissue as captured by the IVIM technique demonstrated a strong correlation with the histological differentiation of HCC.

Specifically, the fifth percentile of the true diffusion coefficient and the skewness of the diffusion map emerged as key differentiators between low-grade and high-grade tumors (17). Poorly differentiated tumors exhibited significantly reduced diffusion values and higher skewness, which are indicative of increased cellular density and heterogeneity. The low diffusion values reflect restricted water mobility within densely packed tumor cells, a hallmark of high cellular proliferation and reduced extracellular space (18). Increased skewness suggests a rightward asymmetric distribution of diffusion values, indicating a substantial proportion of restricted diffusion voxels within the tumor mass. These imaging features are consistent with previous radiological-pathological correlation studies that have reported a progressive decline in diffusion metrics with decreasing histological differentiation.

Our imaging–biomarker phenotype of low D5th (restricted diffusion) combined with elevated AFP, NLR, and CRP aligns with molecular evidence for aggressive cell-cycle dysregulation in HCC. For instance, PSMD12-mediated stabilization of CDK1 accelerates proliferation and migration; such phenotypes are expected to increase tumor cellularity and reduce extracellular space — features effectively captured by lower diffusion percentiles. Similarly, known hepatitis B virus (HBV) mutation patterns (e.g., rtA181T and core-promoter/preS variants) elevate HCC risk and can amplify systemic inflammation, potentially influencing blood-based biomarkers such as NLR and CRP. These mechanistic links support the biological plausibility of our combined signature.

To mitigate confounding, we adjusted for cirrhosis in multivariable analyses and, where available, recorded viral hepatitis status. Future studies will more granularly model HBV-specific factors (including viral load, genotype, and mutation profiles) as covariates or interaction terms, and evaluate whether the IVIM-biomarker model retains its performance across HBV-positive and HBV-negative strata.

Beyond routine serological markers, the addition of molecular markers that track epithelial-mesenchymal transition (EMT), angiogenesis, and metabolic rewiring may further enhance the discrimination of HCC grades. Angiopoietin-like 4 (ANGPTL4) is a secreted protein with context-dependent roles in cancer biology and has been associated with aggressive HCC phenotypes; functional studies indicate that deletion or knockdown of ANGPTL4 reduces HCC cell viability, migration, and invasion in vitro. Clinical studies have also reported elevated circulating ANGPTL4 in liver disease and HCC, supporting the feasibility of serum assays. Given that the low-percentile diffusion metric (D5th) reflects densely cellular, hypoperfused tumor subregions, incorporating a serum ANGPTL4 term may capture complementary biological information. In a prospective cohort, we plan to conduct a nested-model evaluation [ΔAUC with DeLong test, net reclassification improvement (NRI), and integrated discrimination improvement

(IDI)] comparing IVIM plus AFP, NLR, and CRP versus IVIM plus AFP, NLR, CRP, and ANGPTL4, in addition to applying regularized or network-guided feature selection for broader multi-marker panels.

Perfusion-related parameters derived from IVIM imaging also demonstrated diagnostic relevance. The perfusion fraction (f) was significantly lower in poorly differentiated tumors, a finding attributable to the disorganized and dysfunctional neovascular architecture characteristic of aggressive malignancies. High-grade HCC often displays chaotic vasculature, resulting in perfusion heterogeneity and reduced microvascular flow (19, 20). This impairment is reflected in decreased f-values on IVIM maps. Moreover, histogram-based analysis of f-values, particularly at the lower percentiles, provided additional granularity by capturing subtle regional variations within the tumor. These findings underscore the value of whole-volume histogram analysis, which accounts for spatial heterogeneity and avoids the sampling bias inherent in single-region regions of interest (4, 21, 22).

Near-infrared (NIR) activatable probes and fluorescence-guided surgery using indocyanine green (ICG) or next-generation activatable dyes offer high lesion-to-background contrast and real-time visualization of tumor margins, with increasing preclinical and early clinical evidence in HCC. Such agents are particularly valuable intraoperatively for margin assessment and satellite nodule detection; however, most remain investigational, require specialized optical systems, and are not yet widely accessible. By contrast, our imaging-biomarker framework is entirely preoperative, relies on standard MRI and routine laboratory tests, and can be implemented without the need for new tracer approvals. Accordingly, activatable probes serve as

complementary tools for surgical guidance, while our approach targets preoperative biological grading to inform treatment selection and surveillance.

Recent nomograms for predicting portal vein tumor thrombus (PVTT) risk utilize readily available clinical and laboratory variables, offering low-cost, widely applicable tools for preoperative stratification of vascular invasion risk. These models address a related, yet distinct, question — macrovascular invasion — rather than histological differentiation. In clinical practice, a PVTT nomogram can triage risk of vascular involvement, while our IVIM-biomarker model characterizes intratumoral differentiation. Together, these approaches can support surgical candidacy, transplant allocation, and decisions regarding adjuvant strategies. Future work may integrate a PVTT-probability term as a covariate alongside our histogram features and blood markers, yielding a unified risk score encompassing both vascular invasion and tumor grade. Activatable probes, especially those beyond ICG, currently face high costs associated with agent synthesis, regulatory approval, and optical hardware, and their utility is largely confined to intraoperative scenarios. The PVTT nomograms are inexpensive and easy to implement but cannot replace biological grading. Our framework leverages existing diagnostic modalities (MRI and routine laboratory tests), enabling broad adoption with minimal incremental resource requirements. From a health-system perspective, aligning modalities by clinical role — PVTT nomograms for vascular risk, activatable fluorescence for surgical navigation, and IVIM plus biomarkers for biological grading — offers a pragmatic, cost-efficient pathway to improved outcomes without duplicative testing. Prospective health-economic analyses comparing these strategies at key decision points (resection versus ablation versus transplant) are warranted.

In our cohort, interobserver agreement for key histogram metrics was excellent (ICCs ≥ 0.80). However, cross-scanner variability remains a well-recognized challenge for IVIM histogram analysis. Absolute values can vary due to vendor, field strength, b-value sampling, fitting method (mono- versus bi-exponential), motion control, and segmentation strategy, even when relative trends are preserved. We mitigated this by harmonizing 3T acquisition parameters, employing respiratory triggering, whole-lesion segmentation, and z-score normalization, and we observed stable performance during 5-fold cross-validation. For broader implementation, we recommend vendor-agnostic protocols, periodic phantom calibration, and post-hoc feature harmonization (e.g., ComBat) prior to modeling. Looking forward, coupling diffusion histograms with molecularly targeted imaging probes (such as hepatocyte- or angiogenesis-directed contrast agents or activatable probes for surgical correlation) may enhance biological specificity and reduce dependence on absolute IVIM values; however, these approaches entail additional costs and are not yet widely available. Prospective multicenter studies with predefined harmonization protocols and optional probe-based sub-studies are warranted.

In addition to imaging biomarkers, systemic inflammatory markers played a pivotal role in differentiating tumor grades. The NLR, reflecting the balance between pro-inflammatory and anti-tumor immune responses, was significantly higher in patients with poorly differentiated HCC. An elevated NLR indicates a systemic inflammatory state, which has been linked to tumor progression, angiogenesis, and immune evasion. Neutrophils secrete growth factors and matrix-degrading enzymes that facilitate tumor invasion, while lymphopenia signals impaired host immune surveillance. Thus, the NLR serves as a surrogate marker for tumor aggressiveness (22-26).

The CRP, another acute phase reactant, was also elevated in high-grade tumors. Its synthesis is induced by pro-inflammatory cytokines such as interleukin-6, which are commonly upregulated in the tumor microenvironment of aggressive malignancies. Elevated serum CRP levels reflect both tumor-related inflammation and the host's systemic inflammatory response, further supporting its use as a biomarker in cancer grading (27-29).

The AFP, a conventional tumor marker for HCC, also showed a positive correlation with tumor grade. High-grade tumors demonstrated significantly higher AFP levels, consistent with increased proliferative activity and dedifferentiation. Although AFP lacks sensitivity in small or well-differentiated tumors, it remains a valuable component of multiparametric diagnostic strategies (30, 31). The combination of AFP with imaging and inflammatory markers enhances diagnostic specificity and improves stratification of patients for appropriate therapeutic interventions.

The integration of imaging and biomarker data into a multivariate logistic regression model significantly improved the accuracy of tumor grade prediction. The combined model achieved an AUC of the ROC of 0.917, outperforming models based on imaging or biomarkers alone (32-34). This finding underscores the complementary nature of radiological and biochemical markers in capturing distinct aspects of tumor biology. While imaging reflects intratumoral microstructure and perfusion characteristics, systemic biomarkers provide insight into tumor-host interactions and systemic disease manifestations. Their integration allows for a holistic assessment of tumor aggressiveness and facilitates risk stratification.

The high accuracy of the combined model has important clinical implications. Preoperative assessment of tumor grade is essential for treatment planning, especially in patients undergoing liver transplantation or liver-sparing interventions. Poorly differentiated tumors are associated with higher risks of MVI, satellite nodules, and early recurrence following resection or ablation (35). Accurate preoperative identification of such tumors enables clinicians to modify treatment strategies, including the selection of candidates for transplantation, the extent of resection, or the addition of neoadjuvant therapies. Moreover, patients with high-grade tumors may require closer surveillance after treatment due to their aggressive biological behavior.

The robustness of the imaging parameters was supported by strong interobserver agreement. The ICCs for histogram features exceeded 0.80, indicating excellent reproducibility. This is particularly significant for clinical adoption of advanced imaging biomarkers, as reproducibility is a critical requirement for standardization. The use of whole-lesion histogram analysis, rather than manual selection of single slices or hot spots, contributed to this reliability (36). Additionally, the application of respiratory-triggered sequences and harmonized imaging protocols across scanners helped reduce variability, thereby enhancing the generalizability of the proposed method.

This study also addressed the issue of tumor heterogeneity, which is a major challenge in oncology. Tumor heterogeneity may manifest as regional differences in cellularity, necrosis, vascularity, and extracellular matrix composition. Histogram analysis captures this heterogeneity by evaluating the full distribution of pixel-wise parameter values within the tumor volume (37, 38). For example, skewness and kurtosis quantify the asymmetry and peakedness of the parameter distribution, serving as indirect indicators of histological variability. High skewness, as observed in poorly differentiated tumors, suggests dominance of voxels with low diffusion values, possibly reflecting dense cellular foci. These radiomic features are increasingly recognized as imaging surrogates for molecular and genetic heterogeneity and may serve as noninvasive biomarkers for tumor grading, prognosis, and response prediction (39, 40).

Despite these promising results, several limitations must be acknowledged. First, this was a retrospective study and may be subject to potential selection bias. Only patients with available preoperative IVIM imaging and complete laboratory data were included, which may limit generalizability. Second, although imaging protocols were standardized, scanner differences and variations in acquisition techniques may introduce subtle biases. Future prospective multicenter studies with protocol harmonization and external validation are needed to confirm these findings. Third, the sample size of high-grade tumors was relatively small compared to low-grade tumors. Although the statistical power was sufficient to detect significant differences, larger studies are warranted to improve the robustness of subgroup analyses. Another limitation is the exclusion of patients who received neoadjuvant treatment before imaging. While this ensured direct comparability between imaging and histological findings, it also excluded a potentially relevant subset of patients. Including such patients in future studies would enhance the clinical applicability of the model. Additionally, this study did not incorporate advanced radiomic or machine learning techniques beyond histogram analysis. Deep learning models or texture-based approaches may further refine the predictive capability of imaging features and should be considered in future work.

In summary, this study demonstrates that IVIM histogram parameters, when combined with peripheral inflammatory and tumor markers, can accurately predict the pathological differentiation of HCC. This multiparametric approach provides valuable preoperative information that complements traditional imaging assessment and histological evaluation. The high diagnostic accuracy, reproducibility, and biological interpretability of the proposed model support its

potential for integration into clinical workflows. Further prospective validation and incorporation into decision-support systems are needed to facilitate widespread clinical adoption.

5.3. Conclusions

This study provides compelling evidence for the utility of combining IVIM histogram parameters with peripheral blood biomarkers to enhance the preoperative assessment of HCC differentiation. The results demonstrate that diffusion-derived parameters, particularly the fifth percentile and skewness of the true diffusion coefficient, offer robust imaging markers for tumor cellularity and heterogeneity. These imaging findings correlate significantly with tumor grade, reinforcing the biological relevance of IVIM-based metrics. The addition of systemic inflammatory biomarkers such as the NLR and serum AFP levels further strengthens diagnostic performance by capturing tumor–host interactions and systemic disease response.

The integration of imaging and biochemical markers into a predictive model markedly improved the accuracy of differentiating poorly differentiated HCC from well or moderately differentiated types. The combined model exhibited excellent diagnostic performance, with high sensitivity and specificity, providing a practical tool for clinical risk stratification and treatment planning. These findings have direct implications for selecting therapeutic strategies, particularly in liver transplantation, surgical resection, and ablative interventions, where tumor grade plays a decisive role in guiding interventions and predicting recurrence.

The application of histogram analysis to whole-tumor IVIM imaging addresses the challenge of intratumoral heterogeneity and enhances reproducibility, supporting its clinical utility. While further validation through prospective multicenter studies is necessary, this study lays the foundation for the integration of radiomic imaging and blood-based biomarkers into personalized oncology care. In the evolving landscape of HCC diagnostics, this multiparametric, noninvasive approach represents a promising advancement in improving diagnostic precision and optimizing patient outcomes. Future research should focus on prospective multicenter validation to confirm reproducibility across diverse populations and imaging systems. Integration of this combined model with existing clinical nomograms, machine learning, and computational pathology frameworks could further enhance predictive performance and accelerate translation into routine clinical decision-making.

Footnotes

Authors' Contribution: X. Y. conceived and designed the research, analyzed data, drafted, and revised the manuscript critically for important intellectual content. L. W. contributed to the acquisition, analysis, and interpretation of data, and provided substantial intellectual input during the drafting and revision of the manuscript. J. Y. participated in the conception and design of the study and played a key role in data interpretation and manuscript preparation. All authors have read and approved the final version of the manuscript.

Conflict of Interests Statement: The authors declare no conflict of interest.

Data Availability: The data supporting the findings of this study can be obtained from the corresponding author, upon request.

Ethical Approval: Ethical clearance was obtained from the first affiliated hospital of Jinzhou Medical University Institutional Review Boards (ethics approval number: 241054).

Funding/Support: The present study was funded and supported by the Natural Science Foundation of Liaoning Province (grant No.: 2024-MS-198).

References

1. Woo S, Lee JM, Yoon JH, Joo I, Han JK, Choi BI. Intravoxel incoherent motion diffusion-weighted MR imaging of hepatocellular carcinoma: correlation with enhancement degree and histologic grade. *Radiol.* 2014;**270**(3):758-67. [PubMed ID: 24475811]. https://doi.org/10.1148/radiol.13130444.
2. Le Bihan D, Turner R, MacFall JR. Effects of intravoxel incoherent motions (IVIM) in steady-state free precession (SSFP) imaging: application to molecular diffusion imaging. *Magn Reson Med.* 1989;**10**(3):324-37. [PubMed ID: 2733589]. https://doi.org/10.1002/mrm.1910100305.
3. Yoon JH, Lee JM, Baek JH, Shin CI, Kiefer B, Han JK, et al. Evaluation of hepatic fibrosis using intravoxel incoherent motion in diffusion-weighted liver MRI. *J Comput Assist Tomogr.* 2014;**38**(1):110-6. [PubMed ID: 24378888]. https://doi.org/10.1097/RCT.0b013e3182a589be.

4. Granata V, Fusco R, Catalano O, Guarino B, Granata F, Tatangelo F, et al. Intravoxel incoherent motion (IVIM) in diffusion-weighted imaging (DWI) for Hepatocellular carcinoma: correlation with histologic grade. *Oncotarget*. 2016;**7**(48):79357-64. [PubMed ID: 27764817]. [PubMed Central ID: PMC5346719]. https://doi.org/10.18632/oncotarget.12689.
5. Wang T, Li Z, Yu H, Duan C, Feng W, Chang L, et al. Prediction of microvascular invasion in hepatocellular carcinoma based on preoperative Gd-EOB-DTPA-enhanced MRI: Comparison of predictive performance among 2D, 2D-expansion and 3D deep learning models. *Front Oncol*. 2023;**13**:987781. [PubMed ID: 36816963]. [PubMed Central ID: PMC9936232]. https://doi.org/10.3389/fonc.2023.987781.
6. Hoshida Y, Villanueva A, Kobayashi M, Peix J, Chiang DY, Camargo A, et al. Gene expression in fixed tissues and outcome in hepatocellular carcinoma. *N Engl J Med*. 2008;**359**(19):1995-2004. [PubMed ID: 18923165]. [PubMed Central ID: PMC2963075]. https://doi.org/10.1056/NEJMoa0804525.
7. Peng J, Chen H, Chen Z, Tan J, Wu F, Li X. Prognostic value of neutrophil-to-lymphocyte ratio in patients with hepatocellular carcinoma receiving curative therapies: a systematic review and meta-analysis. *BMC Cancer*. 2025;**25**(1):571. [PubMed ID: 40158082]. [PubMed Central ID: PMC11954291]. https://doi.org/10.1186/s12885-025-13972-w.
8. Kinoshita A, Onoda H, Imai N, Iwaku A, Oishi M, Tanaka K, et al. The C-Reactive Protein/Albumin Ratio, a Novel Inflammation-Based Prognostic Score, Predicts Outcomes in Patients with Hepatocellular Carcinoma. *Annals of Surgical Oncology*. 2014;**22**(3):803-10. https://doi.org/10.1245/s10434-014-4048-0.
9. Sterling RK, Wright EC, Morgan TR, Seeff LB, Hoefs JC, Di Bisceglie AM, et al. Frequency of elevated hepatocellular carcinoma (HCC) biomarkers in patients with advanced hepatitis C. *Am J Gastroenterol*. 2012;**107**(1):64-74. [PubMed ID: 21931376]. [PubMed Central ID: PMC3903319]. https://doi.org/10.1038/ajg.2011.312.
10. Lan H, Lin G, Zhong W. A meta-analysis of the added value of diffusion weighted imaging in combination with contrast-enhanced magnetic resonance imaging for the diagnosis of small hepatocellular carcinoma lesser or equal to 2 cm. *Oncol Lett*. 2020;**20**(3):2739-48. [PubMed ID: 32782590]. [PubMed Central ID: PMC7400770]. https://doi.org/10.3892/ol.2020.11805.
11. Podgorska J, Pasicz K, Skrzynski W, Golebiewski B, Kus P, Jasieniak J, et al. Perfusion-Diffusion Ratio: A New IVIM Approach in Differentiating Solid Benign and Malignant Primary Lesions of the Liver. *Biomed Res Int*. 2022;**2022**:2957759. [PubMed ID: 35075424]. [PubMed Central ID: PMC8783718]. https://doi.org/10.1155/2022/2957759.
12. Kakite S, Dyvorne H, Besa C, Cooper N, Facciuto M, Donnerhack C, et al. Hepatocellular carcinoma: short-term reproducibility of apparent diffusion coefficient and intravoxel incoherent motion parameters at 3.0T. *J Magn Reson Imaging*. 2015;**41**(1):149-56. [PubMed ID: 24415565]. https://doi.org/10.1002/jmri.24538.
13. Sokmen BK, Sabet S, Oz A, Server S, Namal E, Dayangac M, et al. Value of Intravoxel Incoherent Motion for Hepatocellular Carcinoma Grading. *Transplant Proc*. 2019;**51**(6):1861-6. [PubMed ID: 31399170]. https://doi.org/10.1016/j.transproceed.2019.02.027.
14. Peng J, Zheng J, Yang C, Wang R, Zhou Y, Tao YY, et al. Intravoxel incoherent motion diffusion-weighted imaging to differentiate hepatocellular carcinoma from intrahepatic cholangiocarcinoma. *Sci Rep*. 2020;**10**(1):7717. [PubMed ID: 32382050]. [PubMed Central ID: PMC7206040]. https://doi.org/10.1038/s41598-020-64804-9.
15. Shao S, Shan Q, Zheng N, Wang B, Wang J. Role of Intravoxel Incoherent Motion in Discriminating Hepatitis B Virus-Related Intrahepatic Mass-Forming Cholangiocarcinoma from Hepatocellular Carcinoma Based on Liver Imaging Reporting and Data System v2018. *Cancer Biother Radiopharm*. 2019;**34**(8):511-8. [PubMed ID: 31314589]. https://doi.org/10.1089/cbr.2019.2799.
16. Wei Y, Gao F, Zheng D, Huang Z, Wang M, Hu F, et al. Intrahepatic cholangiocarcinoma in the setting of HBV-related cirrhosis: Differentiation with hepatocellular carcinoma by using Intravoxel incoherent motion diffusion-weighted MR imaging. *Oncotarget*. 2018;**9**(8):7975-83. [PubMed ID: 29487707]. [PubMed Central ID: PMC5814274]. https://doi.org/10.18632/oncotarget.23807.
17. Wei Y, Gao F, Wang M, Huang Z, Tang H, Li J, et al. Intravoxel incoherent motion diffusion-weighted imaging for assessment of histologic grade of hepatocellular carcinoma: comparison of three methods for positioning region of interest. *Eur Radiol*. 2019;**29**(2):535-44. [PubMed ID: 30027411]. https://doi.org/10.1007/s00330-018-5638-1.
18. Ichikawa S, Motosugi U, Hernando D, Morisaka H, Enomoto N, Matsuda M, et al. Histological Grading of Hepatocellular Carcinomas with Intravoxel Incoherent Motion Diffusion-weighted Imaging: Inconsistent Results Depending on the Fitting Method. *Magn Reson Med Sci*. 2018;**17**(2):168-73. [PubMed ID: 28819085]. [PubMed Central ID: PMC5891343]. https://doi.org/10.2463/mrms.mp.2017-0047.
19. Zhu SC, Liu YH, Wei Y, Li LL, Dou SW, Sun TY, et al. Intravoxel incoherent motion diffusion-weighted magnetic resonance imaging for predicting histological grade of hepatocellular carcinoma: Comparison with conventional diffusion-weighted imaging. *World J Gastroenterol*. 2018;**24**(8):929-40. [PubMed ID: 29491686]. [PubMed Central ID: PMC5829156]. https://doi.org/10.3748/wjg.v24.i8.929.
20. L. I. Mou, Zheng Xing-ju, Huang Zi-xing; et al. [Predicting Histological Grade of HCC in Rats using Intravoxel Incoherent Motion Imaging]. *JOURNAL OF SICHUAN UNIVERSITY (MEDICAL SCIENCES)*. 2018;**49**(2):243-7. ZH.
21. Shan Q, Chen J, Zhang T, Yan R, Wu J, Shu Y, et al. Evaluating histologic differentiation of hepatitis B virus-related hepatocellular carcinoma using intravoxel incoherent motion and AFP levels alone and in combination. *Abdom Radiol*. 2017;**42**(8):2079-88. [PubMed ID: 28337521]. https://doi.org/10.1007/s00261-017-1107-6.
22. Nakanishi M, Chuma M, Hige S, Omatsu T, Yokoo H, Nakanishi K, et al. Relationship between diffusion-weighted magnetic resonance imaging and histological tumor grading of hepatocellular carcinoma. *Ann Surg Oncol*. 2012;**19**(4):1302-9. [PubMed ID: 21927976]. https://doi.org/10.1245/s10434-011-2066-8.
23. Koh DM, Collins DJ, Orton MR. Intravoxel incoherent motion in body diffusion-weighted MRI: reality and challenges. *AJR Am J Roentgenol*. 2011;**196**(6):1351-61. [PubMed ID: 21606299]. https://doi.org/10.2214/AJR.10.5515.
24. Granata V, Fusco R, Filice S, Catalano O, Piccirillo M, Palaia R, et al. The current role and future prospectives of functional parameters by diffusion weighted imaging in the assessment of histologic grade of HCC. *Infect Agent Cancer*. 2018;**13**:23. [PubMed ID: 29988667]. [PubMed Central ID: PMC6029348]. https://doi.org/10.1186/s13027-018-0194-5.
25. Wu B, Jia F, Li X, Li L, Wang K, Han D. Comparative Study of Amide Proton Transfer Imaging and Intravoxel Incoherent Motion Imaging for Predicting Histologic Grade of Hepatocellular Carcinoma. *Front Oncol*. 2020;**10**:562049. [PubMed ID: 33194630]. [PubMed Central ID: PMC7659984]. https://doi.org/10.3389/fonc.2020.562049.
26. Zhou Y, Yang G, Gong XQ, Tao YY, Wang R, Zheng J, et al. A study of the correlations between IVIM-DWI parameters and the histologic

differentiation of hepatocellular carcinoma. *Sci Rep*. 2021;**11**(1):10392. [PubMed ID: 34001962]. [PubMed Central ID: PMC8129092]. https://doi.org/10.1038/s41598-021-89784-2.

27. Song Q, Guo Y, Yao X, Rao S, Qian C, Ye D, et al. Comparative study of evaluating the microcirculatory function status of primary small HCC between the CE (DCE-MRI) and Non-CE (IVIM-DWI) MR Perfusion Imaging. *Abdom Radiol*. 2021;**46**(6):2575-83. [PubMed ID: 33483778]. https://doi.org/10.1007/s00261-020-02945-1.
28. Hussein RS, Tantawy W, Abbas YA. MRI assessment of hepatocellular carcinoma after locoregional therapy. *Insights Imaging*. 2019;**10**(1):8. [PubMed ID: 30694398]. [PubMed Central ID: PMC6352610]. https://doi.org/10.1186/s13244-019-0690-1.
29. Peng J, Yang C, Zheng J, Wang R, Zhou Y, Wang W, et al. Intravoxel Incoherent Motion Diffusion Weighted Imaging for the Therapeutic Response of Transarterial Chemoembolization for Hepatocellular Carcinoma. *J Cancer Ther*. 2019;**10**(7):591-601. https://doi.org/10.4236/jct.2019.107048.
30. Wu LF, Rao SX, Xu PJ, Yang L, Chen CZ, Liu H, et al. Pre-TACE kurtosis of ADC(total) derived from histogram analysis for diffusion-weighted imaging is the best independent predictor of prognosis in hepatocellular carcinoma. *Eur Radiol*. 2019;**29**(1):213-23. [PubMed ID: 29922932]. https://doi.org/10.1007/s00330-018-5482-3.
31. Lin M, Tian M, Zhang W, Xu L, Jin P. Predictive values of diffusion-weighted imaging and perfusion-weighted imaging in evaluating the efficacy of transcatheter arterial chemoembolization for hepatocellular carcinoma. *OncoTargets Ther*. 2016;**Volume 9**:7029-37. https://doi.org/10.2147/ott.S112555.
32. Yang K, Zhang XM, Yang L, Xu H, Peng J. Advanced imaging techniques in the therapeutic response of transarterial chemoembolization for hepatocellular carcinoma. *World J Gastroenterol*. 2016;**22**(20):4835-47. [PubMed ID: 27239110]. [PubMed Central ID: PMC4873876]. https://doi.org/10.3748/wjg.v22.i20.4835.
33. Park YS, Lee CH, Kim JH, Kim IS, Kiefer B, Seo TS, et al. Using intravoxel incoherent motion (IVIM) MR imaging to predict lipiodol uptake in patients with hepatocellular carcinoma following transcatheter arterial chemoembolization: a preliminary result. *Magn Reson Imaging*. 2014;**32**(6):638-46. [PubMed ID: 24703575]. https://doi.org/10.1016/j.mri.2014.03.003.
34. Jia F, Wu B, Yan R, Li L, Wang K, Han D. Prediction Model for Intermediate-Stage Hepatocellular Carcinoma Response to Transarterial Chemoembolization. *J Magn Reson Imaging*. 2020;**52**(6):1657-67. [PubMed ID: 32424881]. https://doi.org/10.1002/jmri.27189.
35. Wu L, Xu P, Rao S, Yang L, Chen C, Liu H, et al. ADC(total) ratio and D ratio derived from intravoxel incoherent motion early after TACE are independent predictors for survival in hepatocellular carcinoma. *J Magn Reson Imaging*. 2017;**46**(3):820-30. [PubMed ID: 28276105]. https://doi.org/10.1002/jmri.25617.
36. Hectors SJ, Lewis S, Kennedy P, Bane O, Said D, Segall M, et al. Assessment of Hepatocellular Carcinoma Response to 90Y Radioembolization Using Dynamic Contrast Material–enhanced MRI and Intravoxel Incoherent Motion Diffusion-weighted Imaging. *Radiol*. 2020;**2**(4). https://doi.org/10.1148/rycan.2020190094.
37. Server S, Sabet S, Bilgin R, Inan N, Yuzer Y, Tokat Y. Intravoxel Incoherent Motion Parameters for Assessing the Efficiency of Locoregional Bridging Treatments before Liver Transplantation. *Transplant Proc*. 2019;**51**(7):2391-6. [PubMed ID: 31474296]. https://doi.org/10.1016/j.transproceed.2019.01.161.
38. Joo I, Lee JM, Han JK, Choi BI. Intravoxel incoherent motion diffusion-weighted MR imaging for monitoring the therapeutic efficacy of the vascular disrupting agent CKD-516 in rabbit VX2 liver tumors. *Radiol*. 2014;**272**(2):417-26. [PubMed ID: 24697148]. https://doi.org/10.1148/radiol.14131165.
39. Wagner M, Doblas S, Daire JL, Paradis V, Haddad N, Leitao H, et al. Diffusion-weighted MR imaging for the regional characterization of liver tumors. *Radiol*. 2012;**264**(2):464-72. [PubMed ID: 22692032]. https://doi.org/10.1148/radiol.12111530.
40. Yang SH, Lin J, Lu F, Han ZH, Fu CX, Lv P, et al. Evaluation of antiangiogenic and antiproliferative effects of sorafenib by sequential histology and intravoxel incoherent motion diffusion-weighted imaging in an orthotopic hepatocellular carcinoma xenograft model. *J Magn Reson Imaging*. 2017;**45**(1):270-80. [PubMed ID: 27299302]. https://doi.org/10.1002/jmri.25344.